

An Efficient Mini-batch Method via Partial Transportation

Khai Nguyen[†] Dang Nguyen[◊] Tung Pham[◊] Nhat Ho[†]

University of Texas, Austin[†]; VinAI Research, Vietnam[◊]

November 15, 2021

Abstract

Mini-batch optimal transport (m-OT) has been widely used recently to deal with the *memory issue* of OT in large-scale applications. Despite their practicality, m-OT suffers from *misspecified mappings*, namely, mappings that are optimal on mini-batch level but do not exist in the optimal transportation plan between the original measures. To address the misspecified mappings issue, we propose a novel mini-batch method by using partial optimal transport (POT) between mini-batch empirical measures, which we refer to as *mini-batch partial optimal transport* (m-POT). Leveraging the insight from the partial transportation, we explain the source of misspecified mappings from the m-OT and motivate why limiting the amount of transported masses among mini-batches via POT can alleviate the incorrect mappings. Finally, we carry out extensive experiments on various applications to compare m-POT with m-OT and recently proposed mini-batch method, mini-batch unbalanced optimal transport (m-UOT). We observe that m-POT is better than m-OT deep domain adaptation applications while having comparable performance with m-UOT. On other applications, such as deep generative model, gradient flow, and color transfer, m-POT yields more favorable performance than both m-OT and m-UOT.

1 Introduction

From its origin in mathematics and economics, optimal transport (OT) has recently become a useful and popular tool in machine learning applications, such as (deep) generative models [2, 40], computer vision/graphics [38, 33], clustering problem [22, 21], and domain adaptation [9, 10, 25]. An important impetus for such popularity is the major advance in computation of OT. In particular, the works of [1, 12, 27] demonstrate that we can approximate optimal transport with a computational complexity upper bound of the order $\mathcal{O}(n^2/\varepsilon^2)$ where n is the maximum number of supports of probability measures and $\varepsilon > 0$ is the desired tolerance. It is a major improvement over to the standard computational complexity $\mathcal{O}(n^3 \log n)$ of computing OT via interior point methods [34]. Another reason for the popularity of optimal transport in machine learning applications are sliced optimal transports [4, 31, 32, 11], which greatly improve the computational complexity of the OT while do not suffer from the curse of dimensionality. The main idea of sliced optimal transport is to project probability measures into a unit sphere and then define proper divergences between these projected probability measures. Sliced optimal transport generally has low computational complexity, which is at the order of $\mathcal{O}(n \log n)$. However, due to the projection step, sliced optimal transport is not able to maintain all important information of high dimensional probability measures, which leads to a decline in practical performance.

Despite of these major improvements on computation, optimal transport and its variants are still challenging to use for large-scale applications when n can be as large as a few millions, such as deep domain adaptation and deep generative model. The challenge mainly comes from the *memory issue*,

namely, we need to store an $n \times n$ cost matrix, which is not practically possible when n is sufficiently large. To deal with that memory issue, practitioners replace the original large-scale computation of OT by cheaper computation on subsets of supports, which widely refer to as mini-batch approaches [19, 39]. In detail, instead of computing the original large-scale optimal transport problem, mini-batch approach splits it into smaller transport problems (sub-problems). Each sub-problem is to solve optimal transport between subsets of supports (or mini-batches), which belongs to the original measures. After we complete solving all the sub-problems, the final transportation cost (plan) is obtained by aggregating evaluated mini-batch transportation costs (plans) from these sub-problems. Due to the small number of samples in each mini-batch, computing transportation plan between mini-batch empirical measures is doable when memory constraints and computational constraints exist. Recently, this mini-batch approach is formulated rigorously under the name of mini-batch optimal transport (m-OT) and some of its statistical properties are investigated in [14, 15].

Despite its practicality, there exists an important limitation of m-OT, which is *misspecified mappings* problem. In particular, a mini-batch is a sparse representation of the original supports; hence, solving an optimal transport problem between empirical mini-batch measures tends to create transport mappings that do not exist in the global optimal transport mappings between the original probability measures. The existence of misspecified mappings had been noticed in [13]. They proposed to use unbalanced optimal transport (UOT) [8] as a replacement of OT for the transportation between mini-batches, which they referred to as mini-batch UOT (m-UOT), and showed that m-UOT can reduce the effect of misspecified mappings from the m-OT. They further provided an objective loss based on m-UOT, which achieves the state-of-the-art results on deep domain adaptation. However, the performance of m-UOT on alleviating the misspecified mappings is not always efficient as the transportation plan from UOT is generally not simple to interpret.

Contributions. In this work, we develop a novel mini-batch framework to alleviate the misspecified matchings issue of m-OT and the interpretability issue of m-UOT. In short, our contributions can be summarized as follows:

1. We propose to use partial optimal transport (POT) between empirical measures formed by mini-batches that can reduce the effect of misspecified mappings and can be more interpretable than m-UOT. The new mini-batch framework, named *mini-batch partial optimal transport* (m-POT), has two practical applications: (i) the first application is efficient mini-batch transportation cost used for objective functions in deep learning problems; (ii) the second application is a meaningful mini-batch transportation plan used for barycentric mappings in color transfer problem. Finally, via some simple examples, we further argue why partial optimal transport (POT) is a natural solution for the misspecified mappings.
2. We conduct extensive experiments on applications that benefit from using mini-batches, including deep domain adaption and deep generative model, to compare m-POT with m-OT and its variant m-UOT [13]. From experimental results, we observe that m-POT is better than m-OT on deep domain adaptation. In particular, m-POT gives at least 0.94 **higher** on the overall accuracy of 12 categories than m-OT. Furthermore, it is comparable to m-UOT on that application, namely, m-POT yields to similar classification accuracy to m-UOT on digit datasets (0.18 **lower** on average accuracy), Office-Home datasets (0.29 **lower** on average accuracy), VisaDA datasets (0.94 **higher** on overall accuracy). On the deep generative model, m-POT provides lower FID scores than m-OT while m-UOT is unstable and difficult to apply

to this application. Finally, experiments on gradient flow and color transfer also demonstrate the favorable performance of m-POT compared to m-OT and m-UOT.

Organization. The paper is organized as follows. In Section 2, we provide backgrounds on (unbalanced) optimal transport and their mini-batch versions. We then highlight limitations of each mini-batch method. In Section 3, we propose mini-batch partial optimal transport to alleviate the limitations of previous mini-batch methods. We describe applications of the proposed mini-batch method to several machine learning applications in Section 4. We provide extensive experiment results of mini-batch POT in Section 5 and conclude the paper with a few discussions in Section 6. Extra experiment results and settings are deferred to the Appendices.

Notation: For α and β are two discrete probability measures $\Pi(\alpha, \beta) := \{\pi \in \mathbb{R}_+^{|\alpha| \times |\beta|} : \pi 1_{|\beta|} = \alpha, \pi^\top 1_{|\alpha|} = \beta\}$ is the set of transportation plans between μ and ν , where $|\alpha|$ denotes the number of supports of α , $\|\alpha\|$ denotes total masses of α . Also, we denote \mathbf{u}_n is the uniform distribution over n supports (similar definition with \mathbf{u}_m). For a set of m samples $X^m := \{x_1, \dots, x_m\}$, P_{X^m} denotes the empirical measures $\frac{1}{m} \sum_{i=1}^m \delta_{x_i}$.

2 Background

In this section, we first restate the definition of Kantorovich optimal transport (OT) and unbalanced Optimal transport (UOT) between two empirical measures. After that, we review the definition of the mini-batch optimal transport (m-OT), mini-batch unbalanced optimal transport (m-UOT), and discuss misspecified matchings issue of m-OT and interpretability issue of m-UOT.

2.1 Optimal Transport and Unbalanced Optimal Transport

Let $\mathcal{X} := \{x_i\}_{i=1}^n$, $\mathcal{Y} := \{y_j\}_{j=1}^n$ be two interested samples. The corresponding empirical measures are denoted by $\mu_n := \frac{1}{n} \sum_{i=1}^n \delta_{x_i}$ and $\nu_n := \frac{1}{n} \sum_{j=1}^n \delta_{y_j}$.

Optimal Transport: The Kantorovich optimal transport [42, 36] between μ_n and ν_n is defined as follows:

$$\text{OT}(\mu_n, \nu_n) := \min_{\pi \in \Pi(\mathbf{u}_n, \mathbf{u}_n)} \langle C, \pi \rangle_F, \quad (1)$$

where C is the distance matrix (or equivalently cost matrix) between \mathcal{X} and \mathcal{Y} that is produced by a ground metric (e.g., Euclidean distance).

Unbalanced Optimal Transport: The unbalanced optimal transport [8] between μ_n and ν_n is defined as follows:

$$\text{UOT}_\phi^\tau(\mu_n, \nu_n) := \min_{\pi} \langle C, \pi \rangle_F + \tau D_\phi(\pi_1, \mu_n) + \tau D_\phi(\pi_2, \nu_n), \quad (2)$$

where C is the distance matrix, $\tau > 0$ is a regularized parameter, D_ϕ is a certain probability divergence (e.g., KL divergence and total variational distance), and π_1, π_2 are respectively the marginal distributions of non-negative measure π and correspond to μ_n, ν_n .

2.2 Mini-batch Optimal Transport

In real applications, the number of samples n is usually very large (e.g., millions). It is due to the large-scale empirical measures or efficient discretization of continuous measures. Therefore, solving directly OT between μ_n and ν_n is generally impractical due to the limitation of computational devices, namely, memory constraints, and vast computation. As a solution, the original n samples of two measures are divided (via sampling with or without replacement) into subsets of m samples, which refer to as mini-batches. The mini-batch size m is often chosen to be the largest number that the computational device can process. Then, a mini-batch framework has the role to aggregate the optimal transport between pairs of the corresponding mini-batches into a final result.

Motivating examples: We now provide some motivating examples to further illustrate the practical importance of mini-batch methods. The first example is regarding training a deep learning model. In practice, it is trained by a loss that requires computing a large-scale OT, e.g., deep generative models [19] and deep domain adaptation [10]. However, due to the limitation of GPU memory, we can only solve OT problems between small mini-batches. The second example is color transfer application, when the numbers of pixels in both source and target images are very large. The mini-batch approach is used to transport a small number of pixels from source images to a small number of pixels from target images [14]. That process is repeated until the histogram of the source images is similar to that of the target.

Now, we will review the definition of mini-batch optimal transport (m-OT) [14, 15]. To ease the ensuing presentation, some notations in that paper are adapted into our paper. To build a mini-batch of $1 \leq m \leq n$ points, we sample $X^m := \{x_1, \dots, x_m\}$ with or without replacement from \mathcal{X}^m (similarly, Y^m are drawn from \mathcal{Y}^m) where m is mini-batch size.

Definition 1. (*Mini-batch Optimal Transport*) For $1 \leq m \leq n$ and $k \geq 1$, X_1^m, \dots, X_k^m and Y_1^m, \dots, Y_k^m are sampled with or without replacement from \mathcal{X}^m and \mathcal{Y}^m respectively. The m-OT transportation cost and transportation plan between μ_n and ν_n are defined as follow:

$$m\text{-OT}_k(\mu_n, \nu_n) = \frac{1}{k} \sum_{i=1}^k OT(P_{X_i^m}, P_{Y_i^m}); \quad \pi^{m\text{-OT}_k} = \frac{1}{k} \sum_{i=1}^k \pi_{P_{X_i^m}, P_{Y_i^m}}^{OT}, \quad (3)$$

where $\pi_{P_{X_i^m}, P_{Y_i^m}}^{OT}$ is a transportation matrix that is returned by solving $OT(P_{X_i^m}, P_{Y_i^m})$. Note that, $\pi_{P_{X_i^m}, P_{Y_i^m}}^{OT}$ is expanded to a $n \times n$ matrix that has padded zero entries to indices which are different from those of X_i^m and Y_i^m .

Misspecified matchings issue of m-OT: m-OT suffers from the problem which we refer to as *misspecified mappings*. In particular, misspecified mappings are non-zero entries in $\pi_k^{m\text{-OT}}$ while they have values of zero in the optimal transport plan π between original measures μ_n and ν_n . To demonstrate this point, we consider the following simple example:

Example 1. Let μ_n, ν_n be two empirical distributions with 5 supports on 2D: $\{(0, 1), (0, 2), (0, 3), (0, 4), (0, 5)\}$ and $\{(1, 1), (1, 2), (1, 3), (1, 4), (1, 5)\}$. The optimal mappings between μ_n and ν_n , $\{(0, i) - (1, i)\}_{i=1}^5$ are shown in Figure 1. Assuming that we use mini-batches of size 3 for m-OT. We specifically consider a pair of mini-batches of samples $X^m = \{(0, 1), (0, 2), (0, 3)\}$ and $Y^m = \{(1, 3), (1, 4), (1, 5)\}$. Solving OT between X^m and Y^m turns into 3 misspecified mappings $(0, 1) - (1, 3)$, $(0, 2) - (1, 4)$, and $(0, 3) - (1, 5)$ that have masses 1/3 (see Figure 1).

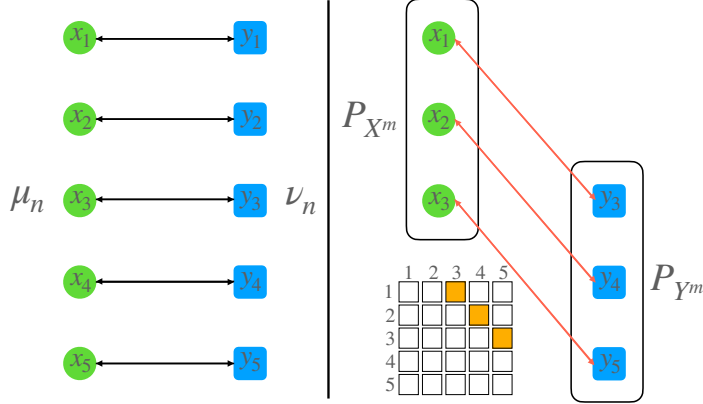


Figure 1: The illustration of Example 1 for m-OT. The green points and blue points are respectively the supports of the empirical measures μ_n and ν_n . Black solid arrows represent the optimal mappings between μ_n and ν_n . Red solid arrows represent misspecified mappings. The 5×5 matrix is the incomplete transportation matrix $\pi_{P_{X^m}, P_{Y^m}}^{\text{OT}}$ which is created from solving OT between P_{X^m} and P_{Y^m} . The boldness of color of arrows and entries of the transportation matrix represents their mass values.

2.3 Mini-batch Unbalanced Optimal Transport

Currently, Fatras et al. [15] had shown that misspecified mappings are caused by transporting all masses between a pair of mini-batches. The reason is that a pair of mini-batches might consists of non-optimal pair of samples. To mitigate the misspecified matchings issue, the authors propose to use unbalanced optimal transport as the transportation type between samples of mini-batches. The mini-batch unbalanced optimal transport is defined as follow:

Definition 2. (*Mini-batch Unbalanced Optimal Transport*) For $1 \leq m \leq n$, $k \geq 1$, $\tau > 0$, a given divergence D_ϕ , X_1^m, \dots, X_k^m and Y_1^m, \dots, Y_k^m are sampled with or without replacement from \mathcal{X}^m and \mathcal{Y}^m respectively. The m -UOT transportation cost and transportation plan between μ_n and ν_n are defined as follow:

$$m\text{-UOT}_k^{\phi, \tau}(\mu_n, \nu_n) = \frac{1}{k} \sum_{i=1}^k \text{UOT}_\phi^\tau(P_{X_i^m}, P_{Y_i^m}); \quad \pi^{m\text{-UOT}_k^{\phi, \tau}} = \frac{1}{k} \sum_{i=1}^k \pi_{P_{X_i^m}, P_{Y_i^m}}^{\text{UOT}_\phi^\tau}, \quad (4)$$

where $\pi_{P_{X_i^m}, P_{Y_i^m}}^{\text{UOT}_\phi^\tau}$ is a transportation matrix that is returned by solving $\text{UOT}_\phi^\tau(P_{X_i^m}, P_{Y_i^m})$. Note that $\pi_{P_{X_i^m}, P_{Y_i^m}}^{\text{UOT}_\phi^\tau}$ is expanded to a $n \times n$ matrix that has padded zero entries to indices which are different from of X_i^m and Y_i^m .

Example: Going back to Example 1, UOT can reduce masses on misspecified matchings by relaxing the marginals of the transportation plan. Using D_ϕ as KL divergence, we show the illustration of m-UOT results in Figure 2. We would like to recall that the regularized coefficient τ controls the degree of the marginal relaxation in m-UOT.

Interpretability issue of m-UOT: Despite being able to alleviate the misspecified mappings issue of m-OT, m-UOT still has some disadvantages. First of all, transportation plan of m-UOT is not easy to interpret since UOT is a marginal relaxation version of OT. Secondly, the performance of

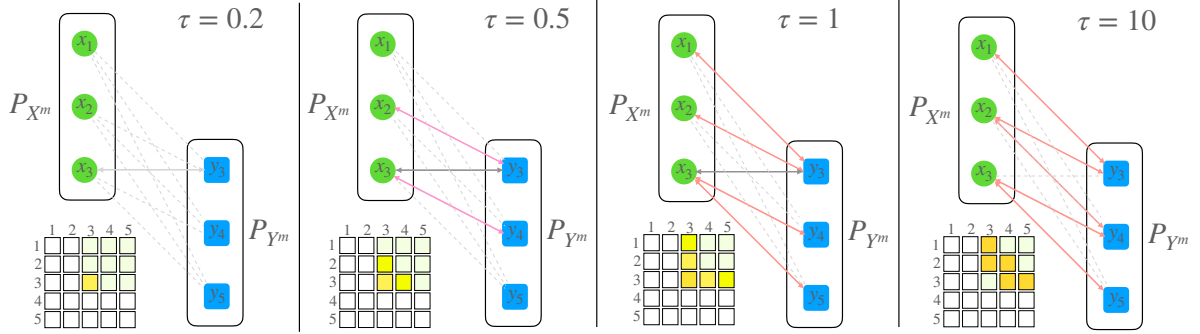


Figure 2: The illustration of Example 1 for m-UOT. As in Figure 1, the green points and blue points are respectively the supports of the empirical measures μ_n and ν_n . Black solid arrows represent the optimal mappings between μ_n and ν_n . Red solid arrows represent misspecified mappings. Dashed arrows are mappings that have very small masses. The parameter τ is the coefficient of the marginal relaxation term of UOT. The 5×5 matrix is the incomplete transportation matrix $\pi_{P_{X^m}, P_{Y^m}}^{\text{UOT}, \tau}$ which is created from solving UOT between P_{X^m} and P_{Y^m} . The boldness of color of arrows and entries of the transportation matrix represent their mass values.

m-UOT depends on the choice of $\tau \in \mathbb{R}^+$ that admits a wide range of value. In addition, the value of τ is also affected by the value of the cost matrix C , e.g., when C contains large values, τ should be respectively large to balance two terms in UOT (see equation (2)). As a result, choosing τ is challenging at some extent. In addition, the transportation plan of UOT tends to have non-zero entries due to the effect of KL divergence (the similar phenomenon tends to occur with other popular divergences that need to use density ratio). Finally, directly solving UOT is not stable and in practice we need to use entropic regularization for a stabler solver [7] (see our experiment results in Section 5 and the Appendices). Because of these weaknesses, it is not convenient to use m-UOT in practical applications and it is non-trivial to explain m-UOT's behaviours when we try to alleviate misspecified matchings.

3 Mini-batch Partial Optimal Transport

To address the misspecified mappings issue of m-OT and interpretability issue of m-UOT, in this section we propose a more explainable mini-batch approach, named *mini-batch partial optimal transport* (m-POT), that uses *partial optimal transport* (POT) as the transportation at the mini-batch level. We first review the definition of partial optimal transport in Section 3.1. Then, we define mini-batch partial optimal transport and discuss its properties in Section 3.2. Moreover, we illustrate that POT is a natural choice of transportation among samples of mini-batches for the mini-batch setting via simple simulations.

3.1 Partial Optimal Transport

Now, we restate the definition of partial optimal transport (POT) that is defined in [17]. Similar to the definition of transportation plans, we define the notion of partial transportation plans. Let $0 < s \leq 1$ which is called transportation fraction, partial transportation plans between two discrete probability measures $\boldsymbol{\alpha}$ and $\boldsymbol{\beta}$ is $\Pi_s(\boldsymbol{\alpha}, \boldsymbol{\beta}) := \{\pi \in \mathbb{R}_+^{|\boldsymbol{\alpha}| \times |\boldsymbol{\beta}|} : \pi 1_{|\boldsymbol{\beta}|} \leq \boldsymbol{\alpha}, \pi^\top 1_{|\boldsymbol{\alpha}|} \leq \boldsymbol{\beta}, 1^\top \pi 1 = s\}$. With previous notations, the partial optimal transport between μ_n and ν_n is defined as follow:

$$\text{POT}_s(\mu_n, \nu_n) = \min_{\pi \in \Pi_s(\boldsymbol{u}_n, \boldsymbol{u}_n)} \langle C, \pi \rangle_F, \quad (5)$$

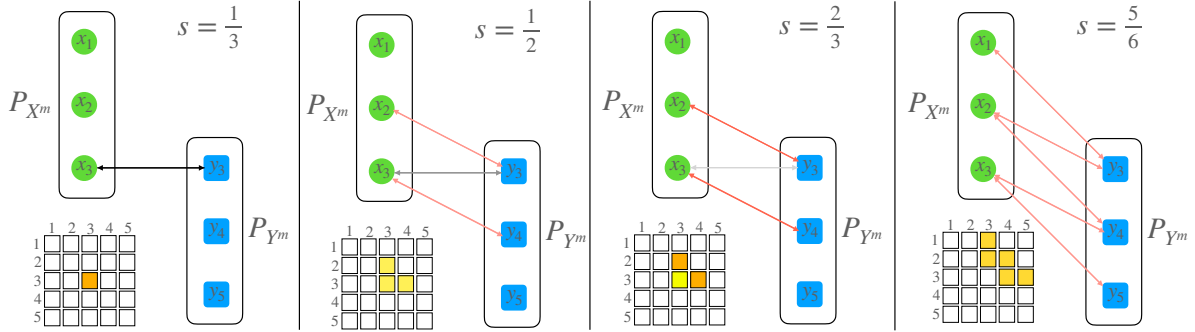


Figure 3: The illustration of Example 1 for m-POT. The meanings of green, blue points and arrows are similar to those in Figure 1. The parameter s is a fraction of masses of POT. The 5×5 matrix is the incomplete transportation matrix $\pi_{P_{X^m}, P_{Y^m}}^{\text{POT}_s}$ which is created from solving POT between P_{X^m} and P_{Y^m} . The boldness of color of arrows and entries of the transportation matrix represent their mass values.

where C is the distance matrix. equation (5) can be solved by adding dummy points (according to [5]) to expand the cost matrix $\bar{C} = \begin{bmatrix} C & 0 \\ 0 & A \end{bmatrix}$, where $A > \|C\|_\infty$. In this case, solving the POT turns into solving the following OT problem:

$$\min_{\pi \in \Pi(\bar{\alpha}, \bar{\alpha})} \langle \bar{C}, \pi \rangle_F, \quad (6)$$

with $\bar{\alpha} = [\mathbf{u}_n, 1 - s]$. Furthermore, the optimal partial optimal transportation plan in equation (5) can be derived from removing the last row and column of the optimal transportation plan π in equation (6).

3.2 Mini-batch Partial Optimal Transport

The partial transportation naturally fits to the mini-batch setting since it is able to decrease the transportation masses of misspecified mappings (cf. the illustration in Figure 3 when two mini-batches contain optimal matching of the original transportation plan). Specifically, reducing the amount of masses to be transported, or reducing s , (from right images to left images in Figure 3) returns globally better mappings. With a right choice of the transport fraction, we can select mappings between samples that are as optimal as doing full optimal transportation. Moreover, POT is also stable to compute since it boils down to OT. Therefore, there are many types of solvers can be utilized to compute POT.

Now, we define *mini-batch partial optimal transport* (m-POT) between μ_n and ν_n as follow:

Definition 3. (*Mini-batch Partial Optimal Transport*) For $1 \leq m \leq n$, $k \geq 1$, $0 < s \leq 1$, X_1^m, \dots, X_k^m and Y_1^m, \dots, Y_k^m are sampled with or without replacement from \mathcal{X}^m and \mathcal{Y}^m respectively. The m-POT transportation cost and transportation plan between μ_n and ν_n are defined as follow:

$$m\text{-POT}_k^s(\mu_n, \nu_n) = \frac{1}{k} \sum_{i=1}^k \text{POT}_s(P_{X_i^m}, P_{Y_i^m}); \quad \pi^{m\text{-POT}_k^s} = \frac{1}{k} \sum_{i=1}^k \pi_{P_{X_i^m}, P_{Y_i^m}}^{\text{POT}_s}, \quad (7)$$

where $\pi_{P_{X_i^m}, P_{Y_i^m}}^{\text{POT}_s}$ is a transportation matrix that is returned by solving $\text{POT}_s(P_{X_i^m}, P_{Y_i^m})$. Note that

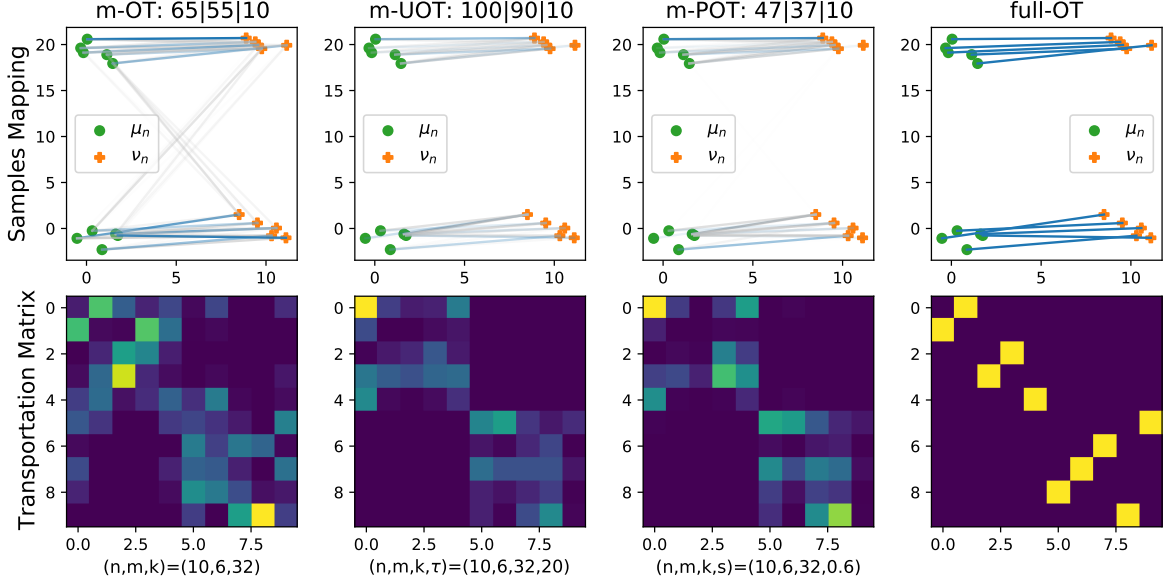


Figure 4: The first row presents sample mappings between μ_n and ν_n from different methods. These mappings are extracted from the transportation matrices which are shown in the second row. Blue lines represent optimal mappings while silver lines represent misspecified mappings. The boldness of the lines and entries of matrices are subject to their masses. There are three numbers near the name of mini-batch methods that are the total number of mappings, the number of misspecified mappings, and the number of optimal mappings respectively.

$\pi_{P_{X_i^m}, P_{Y_i^m}}^{POT_s}$ is expanded to a $n \times n$ matrix that has padded zero entries to indices which are different from of X_i^m and Y_i^m .

Comparison to m-OT and m-UOT: We demonstrate a simulation with 10 supports points drawn from $\frac{1}{2}\mathcal{N}\left(\begin{bmatrix} 0 \\ 0 \end{bmatrix}, \begin{bmatrix} 1 & 0 \\ 0 & 1 \end{bmatrix}\right) + \frac{1}{2}\mathcal{N}\left(\begin{bmatrix} 0 \\ 20 \end{bmatrix}, \begin{bmatrix} 1 & 0 \\ 0 & 1 \end{bmatrix}\right)$ and $\frac{1}{2}\mathcal{N}\left(\begin{bmatrix} 10 \\ 0 \end{bmatrix}, \begin{bmatrix} 1 & -0.8 \\ -0.8 & 1 \end{bmatrix}\right) + \frac{1}{2}\mathcal{N}\left(\begin{bmatrix} 10 \\ 20 \end{bmatrix}, \begin{bmatrix} 1 & -0.8 \\ -0.8 & 1 \end{bmatrix}\right)$ respectively for the empirical measures μ_n and ν_n . We run m-OT, m-UOT (with KL divergence), and m-POT. All methods are run with $k = 32, m = 6$. Then, we visualize the mappings and transportation matrices in Figure 4. For illustration purpose, there are three numbers shown near names of mini-batch approaches. They are the total number of mappings, the number of misspecified mappings, and the number of optimal mappings in turn. We can observe that m-POT and m-UOT provide more meaningful transportation plans than m-OT, namely, masses are put to connections between correct clusters. Importantly, we also observe that m-POT has lower misspecified matchings than m-OT (37 compared to 55). As mentioned in the background section, UOT tends to provide transportation plan that contains non-zero entries; therefore, m-UOT still has many misspecified matchings though the weights of those matchings can be very small that can be ignored in practice. Note that, in the simulation results we select the best value of $\tau \in \{0.1, 0.5, 1, 2, 5, 10, 15, 20, 30, 40, 50\}$ for m-UOT and best value of $s \in \{0.1, 0.2, 0.3, 0.4, 0.5, 0.6, 0.7, 0.8, 0.9\}$ for m-POT.

Computational complexity of m-POT: From the equivalence form of POT in equation (6), we have an equivalent form of m-POT in Definition 3 as follows:

$$m\text{-POT}_k^s(\mu_n, \nu_n) = \frac{1}{k} \sum_{i=1}^k \min_{\pi \in \Pi(\bar{\alpha}_i, \bar{\alpha}_i)} \langle \bar{C}_i, \pi \rangle_F. \quad (8)$$

Here, $\bar{C}_i = \begin{bmatrix} C_i & 0 \\ 0 & A_i \end{bmatrix} \in \mathbb{R}_+^{(m+1) \times (m+1)}$ and $\bar{\alpha}_i = [\mathbf{u}_m, 1 - s]$ where C_i is a cost matrix formed by the differences of elements of X_i^m and Y_i^m and $A_i > \|C_i\|_\infty$ for all $i \in [k]$. The computational complexity of approximating each OT problem in equation (8) is at the order of $\mathcal{O}\left(\frac{(m+1)^2}{\varepsilon^2}\right)$ [27] where $\varepsilon > 0$ is the tolerance. Therefore, the total computational complexity of approximating mini-batch POT is at the order of $\mathcal{O}\left(\frac{k(m+1)^2}{\varepsilon^2}\right)$. It is comparable to the computational complexity of m-OT, which is of the order of $\mathcal{O}\left(\frac{k \cdot m^2}{\varepsilon^2}\right)$ and slightly larger than that of m-UOT, which is of the order of $\mathcal{O}\left(\frac{k \cdot m^2}{\varepsilon}\right)$, in terms of ε .

Practical issue of m-POT: First of all, as indicated in equation (8), m-POT can be converted to m-OT with mini-batch size $m + 1$. Therefore, it is slightly more expensive than m-OT and m-UOT in terms of memory and computation. The second issue of m-POT is the dependence on the choice of fraction of masses s because s plays a vital role in alleviating misspecified mappings from m-OT. At the first glance, choosing s may seem as inconvenient as choosing τ in m-UOT; however, it appears that searching for good s is actually easier than τ . Specifically, the range of s , which is $(0, 1]$, is small compared to that of τ , which is \mathbb{R}^+ .

Discussion on fraction of masses s : First, as indicated in toy examples in Figure 3, choosing small s is a way to mitigate misspecified mappings of m-OT; however, it may also cut off other good mappings when they exist. Therefore, small s tends to require larger number of mini-batches to retrieve enough optimal mappings of the full-OT between original measures. Due to that issue, the fraction of masses s should be chosen adaptively based on the number of good mappings that exists in a pair of mini-batches. In particular, if a pair of mini-batches contains several optimal pairs of samples, s will be set to a high value. Nevertheless, knowing the number of optimal matchings in each pair of mini-batches requires additional information of original large-scale measures. Since designing adaptive algorithm for s is a non-trivial open practical question, we leave this to future work. In this work, we do grid-search for selecting a best value of s for all pairs of mini-batches in our experiments.

4 Applications to Deep Unsupervised Domain Adaption and Deep Generative Model

In this section, we state two popular applications that benefit from using mini-batches, namely, deep domain adaption and deep generative model. We include detailed algorithms for these two applications and the way that we evaluate them. We also investigate the performance of mini-batch methods in other applications, such as color transfer and gradient flow, in Appendix A.

4.1 Mini-batch Deep Domain Adaption

We follow the setting of DeepJDOT [10] that is composed of two parts: an embedding function $G : \mathcal{X} \rightarrow \mathcal{Z}$ which maps data to the latent space; and a classifier $F : \mathcal{Z} \rightarrow \mathcal{Y}$ which maps the latent space to the label space on the target domain. The mini-batch version of DeepJDOT can be expressed as follow, for given the number of mini-batches k and the size of mini-batches m , the goal

Algorithm 1 Mini-batch Deep Domain Adaptation

Input: k, m , source domain (S, Y) , target domain T , chosen $L_{\text{DA}} \in \{L_{\text{OT}}, L_{\text{UOT}}, L_{\text{POT}}\}$
 Initialize G_θ (parametrized by θ), F_ϕ (parametrized by ϕ)
while (θ, ϕ) do not converge **do**
 $\text{grad}_\theta \leftarrow \mathbf{0}$; $\text{grad}_\phi \leftarrow \mathbf{0}$
for $i = 1$ **to** k **do**
 Sample $(s_1, y_1), \dots, (s_m, y_m)$ from (S, Y)
 Sample t_1, \dots, t_m from T
 $S^m \leftarrow \{s_1, \dots, s_m\}; Y^m \leftarrow \{y_1, \dots, y_m\}; T^m \leftarrow \{t_1, \dots, t_m\}$
 Compute $L_{\text{DA}} \leftarrow L_{\text{DA}}(S^m, Y^m, T^m, G_\theta, F_\phi)$
 $\text{grad}_\theta \leftarrow \text{grad}_\theta + \nabla_\theta L_{\text{DA}}$
 $\text{grad}_\phi \leftarrow \text{grad}_\phi + \nabla_\phi L_{\text{DA}}$
end for
 $\theta \leftarrow \text{Adam}(\theta, \text{grad}_\theta)$
 $\phi \leftarrow \text{Adam}(\phi, \text{grad}_\phi)$
end while

is to minimize the following objective function:

$$\min_{G, F} \frac{1}{k} \sum_{i=1}^k L_{\text{OT}_i}; \quad L_{\text{OT}_i} = \left(\frac{1}{m} \sum_{j=1}^m L_s(y_{ij}, F(G(s_{ij}))) + \min_{\pi \in \Pi(\mathbf{u}_m, \mathbf{u}_m)} \langle C_{S_i^m, Y_i^m, T_i^m}^{i, G, F}, \pi \rangle \right), \quad (9)$$

where L_s is the source loss function, S_1^m, \dots, S_k^m are source mini-batches which are sampled with or without replacement from the source domain $S^m \in \mathcal{X}^m$, Y_1^m, \dots, Y_k^m are corresponding labels of S_1^m, \dots, S_k^m , with $S_i^m = \{s_{i1}, \dots, s_{im}\}$ and $Y_i^m := \{y_{i1}, \dots, y_{im}\}$. Similarly, T_1^m, \dots, T_k^m are target mini-batches which are sampled with or without replacement from the target domain $T^m \in \mathcal{X}^m$. The cost matrix $C_{S_i^m, Y_i^m, T_i^m}^{i, G, F}$ denoted C is defined as follows:

$$C_{1 \leq j, t \leq m}^i = \alpha \|G(s_{ij}) - G(t_{it})\|^2 + \lambda_t L_t(y_{ij}, F(G(t_{it}))), \quad (10)$$

where L_t is the target loss function, α and λ_t are hyper-parameters that control two terms.

JUMBOT: By replacing OT to UOT in DeepJDOT, authors in [13] introduce JUMBOT (joint unbalanced mini-batch optimal transport) which achieves the state-of-the-art domain adaptation results on various datasets. Therefore, the objective function in equation (9) turns into:

$$\min_{G, F} \frac{1}{k} \sum_{i=1}^k L_{\text{UOT}_i}; \quad L_{\text{UOT}_i} = \left(\frac{1}{m} \sum_{j=1}^m L_s(y_{ij}, F(G(s_{ij}))) + \min_{\pi} \langle C_{S_i^m, Y_i^m, T_i^m}^{i, G, F}, \pi \rangle \right. \\ \left. + \tau (D_\phi(\pi_1, S_i^m) + D_\phi(\pi_2, T_i^m)) \right), \quad (11)$$

where π_1 and π_2 are marginals of non-negative measure π and respectively correspond to S_i^m and T_i^m .

Deep domain adaptation with m-POT: Similar to JUMBOT, by changing OT into POT with the fraction of masses s , we obtain the following objective loss:

$$\min_{G,F} \frac{1}{k} \sum_{i=1}^k L_{\text{POT}_i}; \quad L_{\text{POT}_i} = \left(\frac{1}{m} \sum_{j=1}^m L_s(y_{ij}, F(G(s_{ij}))) + \min_{\pi \in \Pi_s(\mathbf{u}_m, \mathbf{u}_m)} \langle C_{S_i^m, Y_i^m, T_i^m}^{i, G, F}, \pi \rangle \right), \quad (12)$$

Training Algorithms: We present the algorithm for training domain adaption with m-OT (mini-batch DeepJDOT), m-UOT (JUMBOT), and m-POT in a generalized algorithm which is stated in Algorithm 1.

We utilize Algorithm 1 to compare the performance of m-OT, m-UOT and m-POT. The evaluation criteria is chosen based on the task on domains e.g. classification accuracy on target domain (classification problems).

4.2 Mini-batch Deep Generative Model

We first recall the setting of deep generative models. Given the data distribution $\mu_n := \frac{1}{n} \sum_{i=1}^n \delta_{x_i}$ with $x_i \in \mathcal{X}$, a prior distribution $p(z) \in \mathcal{P}(\mathcal{Z})$ e.g. $p(z) = \mathcal{N}(\mathbf{0}, \mathbf{I})$, and a generator (generative function) $G_\theta : \mathcal{Z} \rightarrow \mathcal{X}$ (where $\theta \in \Theta$ is a neural net). The goal of deep generative model is to find the parameter θ^* that minimizes the discrepancy (e.g. KL divergence, optimal transport distance, etc) between μ_n and $G_\theta \# p(z)$ where the $\#$ symbol denotes the push-forward operator.

Due to the intractable computation of optimal transport distance (n is very large, implicit density of $G_\theta \# p(z)$), mini-batch losses (m-OT, m-UOT, m-POT) are used as surrogate losses to train the generator G_θ . The idea is to estimate the gradient of the mini-batch losses to update the neural network θ . In practice, the real metric space of data samples is unknown, hence, adversarial training is used as unsupervised metric learning [19, 37]. In partial, a discriminator function $F_\phi : \mathcal{X} \rightarrow \mathbb{H}$ where \mathcal{H} is a chosen feature space. The function F_ϕ is trained by maximizing the mini-batch OT loss. For greater detail, the training procedure is described in Algorithm 2.

Evaluation: To evaluate the quality of the generator G_ϕ , we use FID score [20] to compare the closeness of $G_\theta \# p(z)$ to μ_n .

5 Experiments

In this section, we provide experiment results on deep domain adaption (deep DA) and deep generative model (DGM) to compare the performance of m-POT with previous mini-batch approaches, m-OT and m-UOT, and some baseline methods. In Appendix A, we report results of deep DA and DGM in greater details. Also we conduct experiments with gradient flow and color transfer applications to demonstrate further the favorable performance of m-POT in comparison to m-OT and m-UOT. The detailed experimental settings of deep domain adaptation and generative model are in Appendix B.

5.1 Deep Domain Adaptation

In following experiments, we conduct deep domain adaptation on the classification problem. The classification accuracy is utilized to evaluate the mini-batch methods. We first describe the details of datasets that are used in our experiments.

Algorithm 2 Mini-batch Deep Generative Model

```
Input:  $k, m$ , data distribution  $\mu_n$ , prior distribution  $p(z)$ , chosen mini-batch loss  $L_{\text{DGM}} \in \{\text{OT, UOT, POT}\}$ 
Initialize  $G_\theta; F_\phi$ 
while  $\theta$  does not converge do
     $\text{grad}_\theta \leftarrow \mathbf{0}$ 
     $\text{grad}_\phi \leftarrow \mathbf{0}$ 
    for  $i = 1$  to  $k$  do
        Sample  $x_1, \dots, x_m$  from  $\mu_n$ 
        Sample  $z_i, \dots, z_m$  from  $p(z)$ 
        Compute  $y_i, \dots, y_m \leftarrow G_\theta(z_i), \dots, G_\theta(z_m)$ 
         $X^m \leftarrow \{x_1, \dots, x_m\}; Y^m \leftarrow \{y_1, \dots, y_m\}$ 
        Compute  $L_{\text{DGM}}(F_\phi(X^m), F_\phi(Y^m))$ 
         $\text{grad}_\theta \leftarrow \text{grad}_\theta + \theta \phi L_{\text{DGM}}$ 
         $\text{grad}_\phi \leftarrow \text{grad}_\phi - \nabla_\phi L_{\text{DGM}}$ 
    end for
     $\theta \leftarrow \text{Adam}(\theta, \text{grad}_\theta)$ 
     $\phi \leftarrow \text{Adam}(\phi, \text{grad}_\phi)$ 
end while
```

Datasets: We start with Digits datasets. Following the evaluation protocol of [10] we experiment on three adaptation scenarios: SHVN to MNIST ($S \rightarrow M$), USPS to MNIST ($U \rightarrow M$), MNIST to USPS ($M \rightarrow U$). The USPS dataset [23] consists of 7,291 training and 2,007 testing images, each one is a 16×16 grayscale handwritten image. The MNIST dataset [26] contains 60,000 training and 10,000 testing grayscale images of size 28×28 . The SVHN dataset [30] contains house numbers extracted from Google Street View images. This dataset has 73,212 training images, and 26,032 testing RGB images of size 32×32 . Next, we consider Office-Home dataset [41], which is more difficult for domain adaptation. This dataset contains 15,500 in 65 categories from four different domains: artistic (A) paintings, clipart (C), product (P), and real-world (R) images. We evaluate all methods in 12 possible adaptation scenarios. Finally, VisDA-2017 [35] is a large-scale dataset for domain adaptation from synthetic to real images. VisDA consists of 152,397 source (synthetic) images and 55,388 target (real) images. Both source and target domains have the same 12 object categories. Following previous work [29, 6, 13], we evaluate all methods on the validation set. Details about architectures of neural networks and hyper-parameters settings are given in Appendix B.1

Results: We compare our method against state-of-the-art methods: DANN [18], m-OT (DeepJDOT) [10], ALDA [6], and m-UOT (JUMBOT) [13]. We report the best performing checkpoint for all methods. The results on Digits datasets are summarized in Table 1. For fair comparisons, we only resize and normalize the image without data augmentation. Office-Home results are given in Table 2 and VisDA results are gathered in Table 3. We applied a similar data pre-processing and ten-crop technique as in other baselines. We also provide the detailed results for each setting of parameters, e.g., learning rate, the number of mini-batches k , and the fraction of masses s , in all datasets in Tables 4-6 in Appendix A.2.

According to Tables 1-3, m-POT is better than m-OT in all datasets. This phenomenon is expected since m-POT can mitigate the issue of misspecified matchings while m-OT cannot. Compared

Table 1: Summary table of DA results on Digits datasets

Methods	SVHN to MNIST	USPS to MNIST	MNIST to USPS	Avg
m-OT	92.28	96.97	87.59	92.28
m-UOT	99.06	98.75	95.76	97.86
m-POT	98.71	98.58	95.76	97.68

Table 2: Summary table of DA results on Office-Home dataset.

Methods	A2C	A2P	A2R	C2A	C2P	C2R	P2A	P2C	P2R	R2A	R2C	R2P	Avg
DANN	47.81	66.86	74.96	53.11	62.51	65.69	53.19	44.08	74.50	64.85	53.17	79.39	49
ALDA	54.07	74.81	77.28	61.97	71.64	72.96	59.54	51.34	76.57	68.15	56.40	82.11	67.24
m-OT	48.68	65.24	74.41	56.94	64.99	67.20	54.47	46.94	73.03	65.02	54.41	76.73	62.34
m-UOT	54.76	74.23	80.33	65.39	75.40	74.78	65.93	53.79	80.17	73.80	59.47	83.89	70.16
m-POT	54.85	73.51	80.7	65.76	73.62	76.02	64.28	53.5	79.76	74.08	59.22	83.17	69.87

Table 3: Summary of DA results on VisDA dataset.

Methods	Accuracy
DANN	68.09
ALDA	71.38
m-OT	55.21
m-UOT	71.52
m-POT	72.46

to m-UOT, m-POT is comparable in digits datasets and Office-Home datasets, namely, m-POT gives only 0.18 lower accuracy (average) on digits datasets and 0.29 lower accuracy (average) on Office-Home datasets. In contrast, on VisDA dataset, m-POT gives higher accuracy than m-UOT (72.46 compared to 71.52). Note that, we reproduced the results for baseline methods and reported them instead of using their reported performance in the corresponding papers. Although our results do not match their reported numbers, we still manage to have some better results than those in their papers. For Digits datasets, m-OT achieved higher accuracy on USPS to MNIST scenario while m-UOT got better performance on both SVHN to MNIST and USPS to MNIST. For Office-Home dataset, m-OT had higher accuracies in 12 out of 12 scenarios. ALDA and m-UOT achieved better performance in 8 and 6 scenarios, respectively.

The role of s : We demonstrate the effect of choosing s in m-POT. We observe a general pattern in all figures as follows. When s increases to the optimal mass, the accuracy also increases. After that, the accuracy drops as s goes further from the optimal value. As discussed in Section 3, the right value of s is important in making m-POT to perform well. In Figure 5, we show the accuracy of different values of s on all datasets. From that figure, the best value of s is the value that is not too big and not too small. The reason is that a large value of s creates more misspecified matchings while a small value of s might drop off too many mappings. The latter leads to lazy gradient, thus slower the learning process.

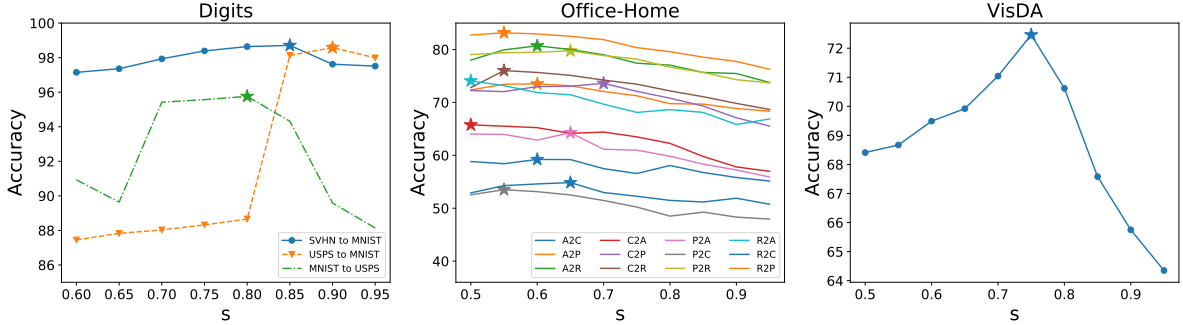


Figure 5: Performance of m-POT on DA when changing mass size s . The optimal masses s , which achieve the best accuracy, are marked by \star symbol. In the left figure, the optimal masses for Digits datasets lie between 0.8 and 0.9. In the middle figure, the best performing masses are smaller, from 0.5 to 0.7. On the VisDA dataset in the right figure, the optimal mass s is 0.75.

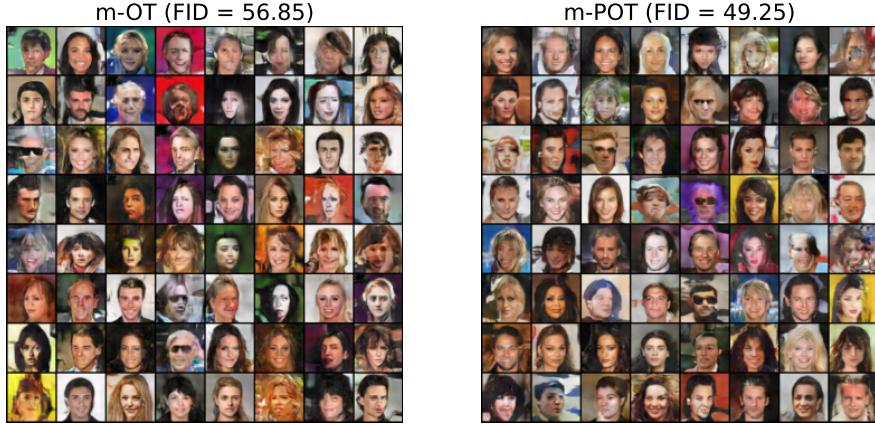


Figure 6: CelebA generated images from different mini-batch losses, $(k, m) = (2, 200)$. With the same settings, m-POT improves the FID score of m-OT with a margin of 7.6 point.

5.2 Deep Generative Model

We now review about datasets that we trained generators on.

Datasets: We train generators on CIFAR10 [24] and CelebA [28] datasets. The CIFAR10 dataset contains 10 classes, with 50,000 training and 10,000 testing color images of size 32×32 . CelebA is a large-scale face attributes dataset with more than 200K celebrity images. We describe the neural network architectures and the used parameters in Appendix B.2.

Results: By evaluating the FID score, we observe that m-POT yields better generators than m-OT on both CIFAR10 and CelebA. The qualitative results (randomly generated images) and the corresponding FID scores of m-OT and m-POT on CelebA datasets are given in Figure 6. Generated images and FID scores on CIFAR10 are presented in Figure 8 in Appendix A.3. On the comparison with m-UOT, we have not been able to achieve a good enough setting for m-UOT (a good enough setting means a setting that can provide a generative network that can generate reasonable images). To our best knowledge, there are not any generative models that are implemented with m-UOT, hence, we leave this comparison to future works.

On debiased mini-batch energy: Both m-OT and m-POT can be extended to debiased energy versions based on the work [37]. However, in this paper, we want to solely focus on the effect of misspecified matchings on applications, hence, we choose to use the original mini-batch losses.

6 Discussion

In this paper, we have introduced a novel mini-batch approach that is referred to as mini-batch partial optimal transport (m-POT). The new mini-batch approach can address the issue of misspecified mappings in the conventional mini-batch optimal transport approach and also provides an interpretable framework to understand such types of wrong matchings. Moreover, we also observe that m-POT is easier than mini-batch unbalanced optimal transport in choosing hyper-parameter. Finally, via extensive experiment studies, we demonstrate that m-POT is comparable to m-UOT in deep domain adaptation while it is better than m-OT in this application. Furthermore, in other applications, including deep generative model, color transfer, and gradient flow, m-POT is better than both m-OT and m-UOT. There are a few natural future directions arising from our work: (i) first, we will develop efficient algorithms to choose the fraction of masses s of m-POT adaptively; (ii) second, we would like to explore further the dependence structure between mini-batches and implement m-POT in more large-scale experiments.

7 Acknowledgements

This work was partially supported by the Institute for Foundations of Machine Learning (IFML) grant to NH.

Supplement to "An Efficient Mini-batch Method via Partial Transportation"

In this supplement, we provide additional experimental results in Appendix A. In particular, we show detailed results on deep domain adaptation in Appendix A.2, deep generative model in Appendix A.3. Moreover, we conduct experiments on color transfer application and gradient flow application to show the favorable performance of m-POT in Appendix A.4 and Appendix A.5 respectively. Finally, we report the experimental settings including neural network architectures, hyper-parameter choices in Appendix B.

A Additional experiments

We first provide an additional simulation for demonstrating the role of s in m-POT in Appendix A.1. We then show tables that contain results of all run settings in domain adaptation in Appendix A.2. Then, we report the deep generative model experiments on CIFAR10 in Appendix A.3. Finally, we report results on color transfer and gradient flow in Appendices A.4 and A.5 respectively.

A.1 Transportation Matrix

Here, we repeat the simulation in the main text with two empirical measures of 10 samples. The difference is that we run only m-POT with the value of fraction of masses $s \in \{0.2, 0.4, 0.6, 0.8\}$. It

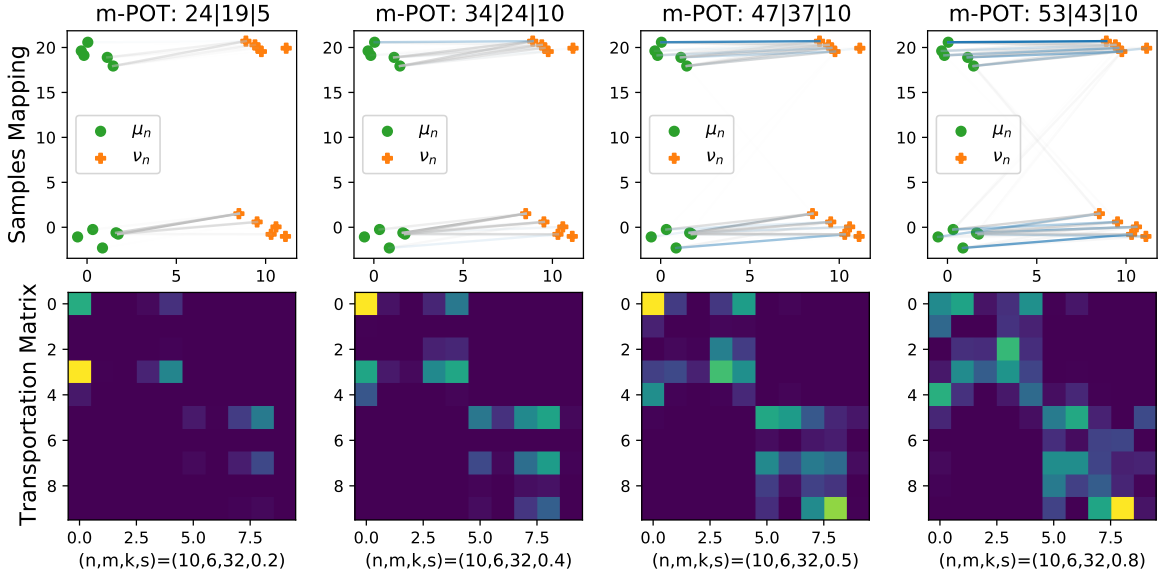


Figure 7: The first row presents sample mappings between μ_n and ν_n from different methods. These mappings are extracted from the transportation matrices which are shown in the second row. Blue lines represent optimal mappings while silver lines represent misspecified mappings. The boldness of the lines and entries of matrices are subject to their masses. There are three numbers near the name of mini-batch methods that are the total number of mappings, the number of misspecified mappings, and the number of optimal mappings respectively.

is easy to see that a smaller value of s leads to a smaller number of misspecified mappings. However, a small value of s also removes good mappings (e.g. $s = 0.2$ only has 5 correct mappings). With the right choice of s (e.g. $s = 0.4$ and $s = 0.5$), we can obtain enough good mappings while having a reasonable number of misspecified matchings.

A.2 Deep Domain Adaptation Experiments

We first want to emphasize that we have used the best parameters settings for m-UOT that are reported in [13] in each experiment.

We observe that m-POT outperforms m-OT in all digit datasets (see in Table 4). Compared to m-UOT, m-UOT is slightly better than m-POT in adaptation from SVHN to MNIST, and USPS to MNIST. On the other hand, m-POT is slightly better than m-UOT on MNIST-USPS adaptation. In general, we can conclude that m-UOT and m-POT are similar in terms of classification accuracy. In addition, a higher learning rate usually leads to higher accuracy in m-UOT and m-POT, this is not the case for m-OT. Because m-UOT and m-POT have smaller gradient update per step than that of m-OT, they require more steps or higher learning rates.

According to Table 5, m-POT is still much better than m-OT on Office-Home datasets. Also, we observe that m-POT and m-UOT provide similar numbers of classification accuracy. When the source domain is synthetic (A and C), m-POT performs better than m-UOT in two-third of scenarios. When the source domain is real (P and R), m-UOT achieves more favorable results except for the case of R2A. We also notice that m-UOT is always better than m-POT when either source or target domain is Product.

Table 4: Details of DA results on Digits datasets.

	k	LR	m-OT	m-UOT	m-POT(0.6)	m-POT(0.65)	m-POT(0.7)	m-POT(0.75)	m-POT(0.8)	m-POT(0.85)	m-POT(0.9)	m-POT(0.95)
S → M	1	0.0002	92.21	98.72	96.33	97.36	97.57	97.87	97.61	97.24	97.45	96.17
		0.0003	92.28	98.95	96.52	97.07	97.42	98.26	98.4	97.88	96.86	97.51
		0.0004	92.17	99.06	96.86	97.09	97.80	98.14	97.69	98.71	97.28	95.96
	2	0.0002	90.00	98.83	97.02	97.25	97.93	97.01	98.46	97.55	97.13	93.48
		0.0003	88.85	98.89	97.15	97.14	97.80	98.39	98.63	98.66	97.42	93.71
		0.0004	89.44	99.03	96.99	97.29	97.70	97.09	98.64	98.09	97.62	94.43
U → M	1	0.0002	96.72	97.12	80.82	87.17	87.68	87.96	88.20	97.71	97.85	97.80
		0.0003	96.88	98.63	86.50	87.42	87.85	88.13	88.47	97.90	98.06	97.99
		0.0004	96.97	98.75	86.76	87.67	87.97	88.32	88.57	97.93	98.20	97.93
	2	0.0002	96.90	97.42	80.12	87.66	87.85	88.05	88.66	97.99	98.24	97.64
		0.0003	96.95	97.47	81.13	87.75	87.91	88.15	88.47	98.05	98.45	97.61
		0.0004	96.90	98.28	87.45	87.83	88.03	88.21	88.59	98.13	98.58	97.68
M → U	1	0.0002	86.95	95.47	90.53	88.04	95.02	95.52	93.82	89.49	88.14	
		0.0003	87.05	95.57	90.83	89.64	95.07	95.17	95.42	93.82	89.59	87.64
		0.0004	85.80	95.47	90.93	89.64	95.07	95.22	95.52	94.32	89.24	87.74
	2	0.0002	87.59	95.67	87.94	87.74	95.27	95.57	95.67	93.32	88.74	87.19
		0.0003	86.85	95.67	89.44	87.89	95.42	95.47	95.76	93.22	88.69	87.79
		0.0004	86.90	95.76	90.58	87.79	95.37	95.52	95.76	93.42	89.29	87.49

Table 5: Details of DA results on Office-Home dataset.

Methods	A2C	A2P	A2R	C2A	C2P	C2R	P2A	P2C	P2R	R2A	R2C	R2P
DANN	47.81	66.86	74.96	53.11	62.51	65.69	53.19	44.08	74.50	64.85	53.17	79.39
ALDA	54.07	74.81	77.28	61.97	71.64	72.96	59.54	51.34	76.57	68.15	56.40	82.11
m-OT	48.68	65.24	74.41	56.94	64.99	67.20	54.47	46.94	73.03	65.02	54.41	76.73
m-UOT	54.76	74.23	80.33	65.39	75.40	74.78	65.93	53.79	80.17	73.80	59.47	83.89
m-POT(0.5)	52.90	72.36	78.00	65.76	72.25	72.80	64.03	52.53	79.05	74.08	58.83	82.74
m-POT(0.55)	54.27	73.44	79.94	65.51	72.04	76.02	63.95	53.50	79.40	73.18	58.42	83.17
m-POT(0.6)	54.59	73.51	80.70	65.23	72.99	75.67	62.88	53.13	79.48	71.86	59.22	82.95
m-POT(0.65)	54.85	73.15	80.01	64.15	73.06	75.12	64.28	52.51	79.76	71.45	59.20	82.50
m-POT(0.7)	52.97	72.07	79.02	64.40	73.62	74.23	61.15	51.46	78.86	69.67	57.48	81.87
m-POT(0.75)	52.26	71.26	77.42	63.49	72.09	73.45	60.98	50.22	78.20	68.11	56.56	80.36
m-POT(0.8)	51.48	69.77	77.05	62.26	70.80	72.18	59.83	48.50	76.66	68.64	58.08	79.59
m-POT(0.85)	51.18	69.68	75.67	59.79	69.32	71.08	58.34	49.26	75.67	68.11	56.75	78.56
m-POT(0.9)	51.89	68.85	75.47	57.81	67.09	69.82	57.23	48.32	74.30	65.84	55.81	77.74
m-POT(0.95)	50.75	68.35	73.77	56.98	65.53	68.67	55.91	47.95	73.70	66.87	55.14	76.28

Table 6: Details of DA results on VisDA dataset.

Methods	All	plane	bcycl	bus	car	house	knife	mcycl	person	plant	sktbrd	train	truck	Avg
DANN	68.09	85.77	91.41	67.57	68.25	91.39	9.79	59.99	78.86	72.40	37.92	61.47	47.40	64.35
ALDA	71.38	95.15	96.61	68.28	70.77	91.39	9.21	61.26	78.77	75.50	39.38	70.57	69.34	68.85
m-OT	55.21	59.49	87.44	69.06	68.24	78.19	19.54	44.96	55.66	62.33	21.75	46.54	41.37	54.55
m-UOT	71.52	97.07	94.00	64.19	74.69	91.40	7.06	65.49	74.88	84.83	40.28	64.66	45.39	67.00
m-POT(0.5)	68.41	80.64	91.86	81.27	64.96	88.15	51.90	67.98	67.00	66.97	30.33	57.49	56.89	67.12
m-POT(0.55)	68.67	84.71	94.47	72.98	67.04	90.49	53.57	64.84	65.79	68.30	29.81	61.51	64.29	68.15
m-POT(0.6)	69.49	82.33	93.57	72.09	69.81	86.67	66.03	67.07	65.98	68.26	28.81	60.47	70.10	69.27
m-POT(0.65)	69.92	82.31	93.89	71.37	70.63	88.21	69.44	67.38	63.59	71.43	29.74	60.46	68.50	69.75
m-POT(0.7)	71.04	85.92	92.63	75.10	72.37	89.08	88.55	58.05	68.57	76.65	29.64	62.17	80.97	73.31
m-POT(0.75)	72.46	87.22	92.23	72.74	76.15	92.41	74.11	59.87	71.53	74.89	35.28	62.80	71.83	72.59
m-POT(0.8)	70.62	82.40	91.61	64.31	69.41	92.65	70.18	61.98	70.95	76.10	27.60	65.96s	53.02	68.85
m-POT(0.85)	67.58	71.53	92.33	67.19	70.16	90.93	7.42	71.76	74.36	72.23	24.75	52.88	36.73	61.02
m-POT(0.9)	65.75	93.44	83.76	64.78	73.35	84.72	4.83	58.64	75.27	69.60	27.92	49.89	43.93	60.84
m-POT(0.95)	64.35	79.21	80.31	65.71	64.90	74.95	61.04	53.03	66.13	78.66	24.48	60.03	20.61	60.76

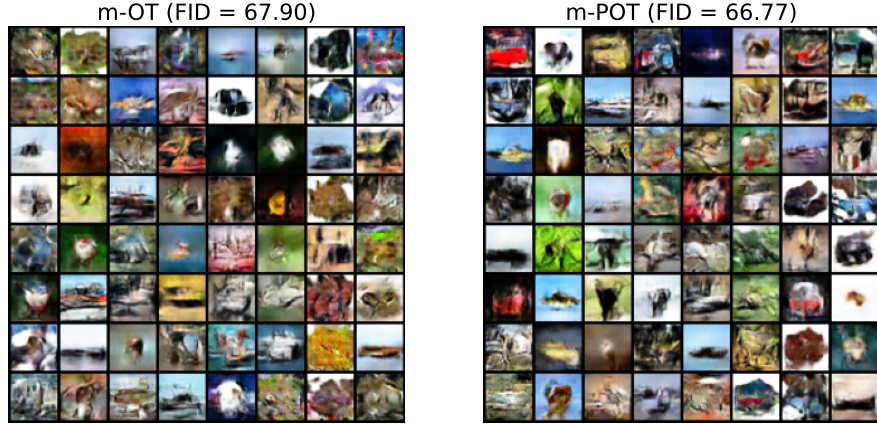


Figure 8: CIFAR10 generated images from different mini-batch losses, $(k,m) = (2,100)$. With the same settings, m-POT improves the FID score of m-OT with a margin of 1.13 point.

Table 6 illustrates that m-POT yields the best performance in 6 out of 12 categories. Knife is a difficult category in which other baselines only achieve less than 20% accurate prediction. However, m-POT has an accuracy of 88.55%, which creates a large margin of nearly 70%. m-POT also leads to a significant margin (4.46%) of the average class accuracy.

A.3 Deep Generative Model Experiments

OT has been widely utilized to measure the discrepancy between a parametric distribution and real data distribution in a generative model. In this experiment, we apply m-OT and m-POT into the deep generative model. We reported the best performing checkpoint, which was measured by FID score, along with their generated images from random noise. The generated images and the corresponding FID scores of m-OT and m-POT on CIFAR10 datasets are given in Figure 8. m-POT leads to a slight improvement over m-OT in terms of FID score.

A.4 Color Transfer

In this section, we first state the color transfer algorithm [14] that we used to compare mini-batch methods in Algorithm 3 .

Results: We show some transferred images from the m-OT and m-POT with two values of s (0.9 and 0.99) in Figure 9. We observe that m-POT with the right choice of parameter s generates more beautiful images than the m-OT. We have tried to run UOT in this application, however, we have not found the setting that UOT can provide reasonable results yet.

Algorithm 3 Color Transfer with mini-batches

Input: k, m , source domain $X_s \in \mathbb{R}^{n \times d}$, target domain $X_t \in \mathbb{R}^{n \times d}$, $T \in \{\text{OT}, \text{UOT}, \text{POT}\}$
 Initialize $Y_s \in \mathbb{R}^{n \times d}$
 Initialize $M \in \mathbb{R}^{k \times k}$
for $i = 1$ **to** k **do**
 Select set A of m samples in X_s
 Select set B of m samples in X_t
 Compute the cost matrix $C_{A,B}$
 $\pi \leftarrow T(\langle C_{A,B}, \pi \rangle)$
end for
 $Y_s|_{A_{ij}} \leftarrow Y_s|_A + \pi \cdot X_t|_B$
Output: Y_s

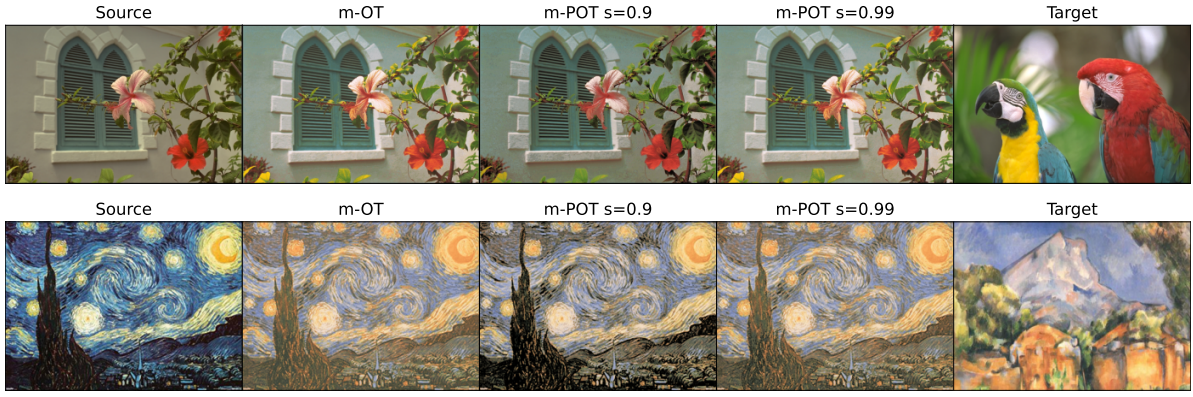


Figure 9: Color Transfer results from m-OT, m-POT with $k = 320, m = 32$. The leftmost image is the source image and the rightmost image is the target image. In between images transferred images with the corresponding name of the method on top.

A.5 Gradient Flow

In this appendix, we describe the gradient flow application and the usage of mini-batch methods in this case.

Gradient flow is a non-parametric method to learn a generative model. The goal is to find a distribution μ that is close to the data distribution ν in sense of a discrepancy D . So, a gradient flow can be defined as:

$$\partial_t \mu_t = -\nabla_{\mu_t} D(\mu_t, \nu) \quad (13)$$

We follow the Euler scheme to solve this equation as in [16], starting from an initial distribution at time $t = 0$. In this paper, we consider using mini-batch losses such as m-OT, m-UOT, and m-POT as the discrepancy D .

We compare m-OT, m-UOT, and m-POT in a toy example as in [16] and present our results in Figure 10. In short, we want to move the colorful empirical measure to the "S-shape" measure. Each measure has 1000 support points. Here, we choose $(k, m) = (4, 4)$ and learning rate is set to 0.001. We use entropic regularization [7] to solve m-UOT, we choose the best entropic regularization

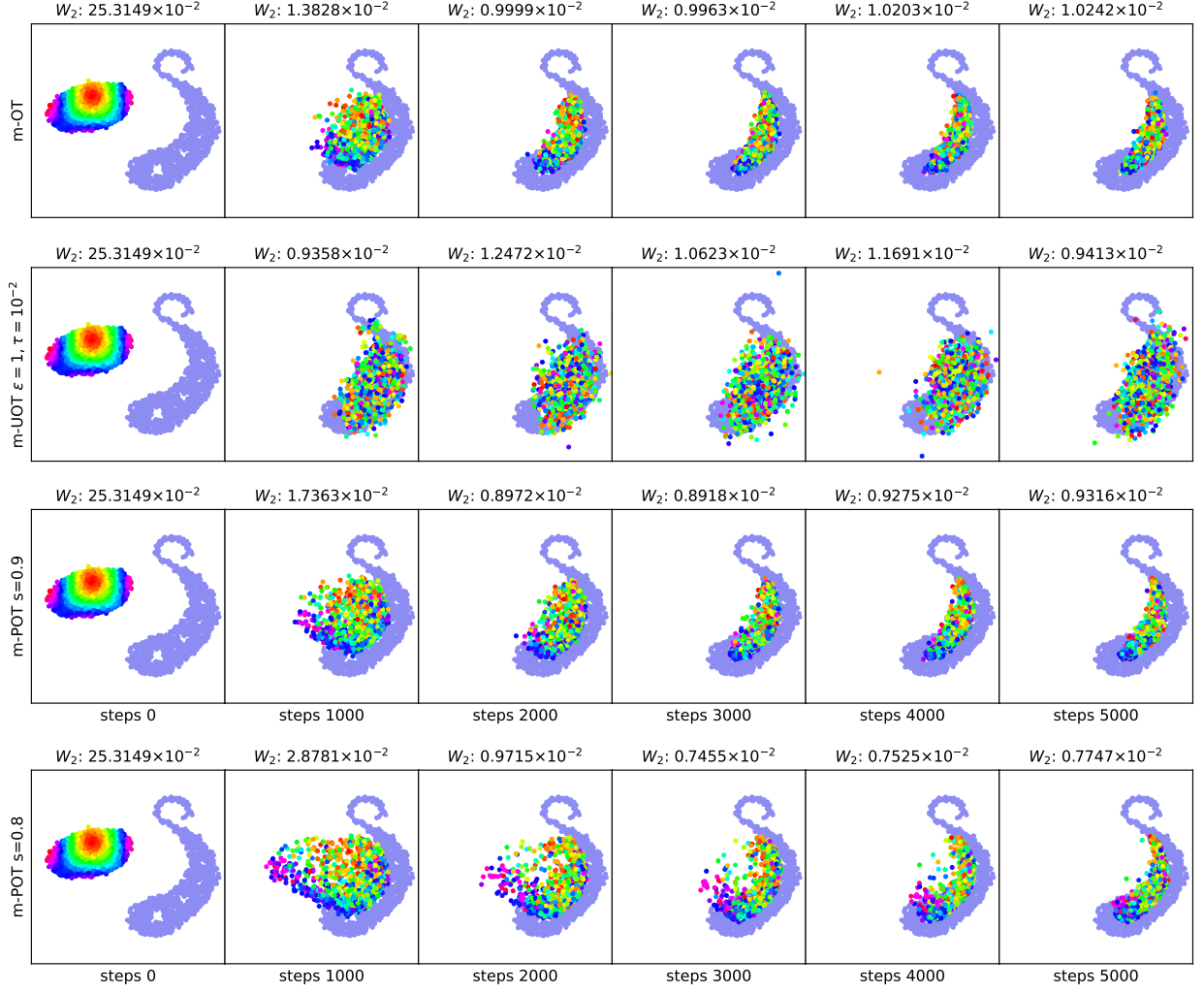


Figure 10: Gradient flows from different mini-batch methods. The Wasserstein-2 distance between two measures in each step is reported at the top of the corresponding image.

parameter $\epsilon \in \{0.1, 1, 2, 5, 10\}$ and marginal relaxation parameter $\tau \in \{0.001, 0.01, 0.1, 1, 2, 5, 10\}$. From the figure, we observe that m-POT yields better flows than both m-OT and m-UOT, namely, the final Wasserstein-2 score of m-POT is the lowest. Interestingly, we see that reducing the amount of masses s in m-POT from 0.9 to 0.8 improves considerably the result.

B Experimental Settings

In this section we provide architecture and training procedure details for domain adaptation and generative model.

B.1 Deep Domain Adaptation

Similar to DeepJDOT [3] and JUMBOT [13], we stratified the data loaders so that each class has the same number of samples in the mini-batches. For Digits datasets, we also trained our neural network on the source domain during 10 epochs before applying our method.

Digits datasets: Following DeepJDOT and JUMBOT, we used CNN for our generator and 1 FC layer for our classifier. We optimized using Adam with the initial learning rate of 0.0002. We trained all algorithms with a batch size of 500 during 100 epochs. The hyperparameters in equation (10) follow the settings in m-UOT: $\alpha = 0.1$, $\lambda_t = 0.1$. For computing UOT, we also set τ to 1 and ϵ to 0.1.

Generator architecture was used for SVHN dataset:

$$z \in \mathbb{R}^{32 \times 32 \times 3} \rightarrow \text{Conv}_{32} \rightarrow \text{BatchNorm} \rightarrow \text{ReLU} \rightarrow \text{Conv}_{32} \rightarrow \text{BatchNorm} \rightarrow \text{ReLU} \rightarrow \text{MaxPool2D} \rightarrow \text{Conv}_{64} \rightarrow \text{BatchNorm} \rightarrow \text{ReLU} \rightarrow \text{Conv}_{64} \rightarrow \text{BatchNorm} \rightarrow \text{ReLU} \rightarrow \text{MaxPool2D} \rightarrow \text{Conv}_{128} \rightarrow \text{BatchNorm} \rightarrow \text{ReLU} \rightarrow \text{Conv}_{128} \rightarrow \text{BatchNorm} \rightarrow \text{ReLU} \rightarrow \text{MaxPool2D} \rightarrow \text{Sigmoid} \rightarrow \text{FC}_{128}$$

Generator architecture was used for USPS dataset:

$$z \in \mathbb{R}^{28 \times 28 \times 3} \rightarrow \text{Conv}_{32} \rightarrow \text{BatchNorm} \rightarrow \text{ReLU} \rightarrow \text{MaxPool2D} \rightarrow \text{Conv}_{64} \rightarrow \text{BatchNorm} \rightarrow \text{ReLU} \rightarrow \text{Conv}_{128} \rightarrow \text{BatchNorm} \rightarrow \text{ReLU} \rightarrow \text{MaxPool2D} \rightarrow \text{Sigmoid} \rightarrow \text{FC}_{128}$$

Classifier architecture was used for both SVHN and USPS datasets:

$$z \in \mathbb{R}^{128} \rightarrow \text{FC}_{10}$$

For Office-home and VisDA, our generator is a ResNet50 pre-trained on ImageNet except for the last FC layer, which is our classifier. As we train the classifier from scratch, we set their learning rates to be 10 times that of the generator. We train the models with an SGD optimizer with momentum = 0.9 and weight decay = 0.0005. We schedule the learning rate with the same strategy used in [18]. The learning rate at iteration p is $\eta_p = \frac{\eta_0}{(1+\mu q)^\nu}$, where q is the training progress linearly changing from 0 to 1, $\eta_0 = 0.01$, $\mu = 10$, $\nu = 0.75$.

Office-home dataset: We trained all algorithms with a batch size of 65 during 10000 iterations. Following m-UOT, the hyperparameters for computing the cost matrix is as follows $\alpha = 0.01$, $\lambda_t = 0.5$, $\tau = 0.5$, $\epsilon = 0.01$.

Classifier architecture was used for Office-Home dataset:

$$z \in \mathbb{R}^{512} \rightarrow \text{FC}_{65}$$

VisDA dataset: We trained all algorithms with a batch size of 72 during 10000 iterations. The hyperparameters for computing the cost matrix is as follows $\alpha = 0.005$, $\lambda_t = 1$, $\tau = 0.3$, $\epsilon = 0.01$.

Classifier architecture was used for both VisDA datasets:

$$z \in \mathbb{R}^{512} \rightarrow \text{FC}_{12}$$

B.2 Deep Generative Model

FID scores: We use 10000 samples from the generative model and all images from the training set to compute FID score by the official code from authors in [20].

Parameter settings: We chose a learning rate equal to 0.0005, mini-batch size equal to 200 for CelebA and 100 for CIFAR10. The number of epochs is set to 200 in both datasets.

Neural network architectures: We used CNNs for both generators and discriminators on the CelebA and CIFAR10 datasets.

Generator architecture was used for CelebA:

$$z \in \mathbb{R}^{128} \rightarrow \text{TransposeConv}_{512} \rightarrow \text{BatchNorm} \rightarrow \text{ReLU} \rightarrow \text{TransposeConv}_{256} \rightarrow \text{BatchNorm} \rightarrow \text{ReLU} \rightarrow \text{TransposeConv}_{128} \rightarrow \text{BatchNorm} \rightarrow \text{ReLU} \rightarrow \text{TransposeConv}_{64} \rightarrow \text{BatchNorm} \rightarrow \text{ReLU} \rightarrow \text{TransposeConv}_3 \rightarrow \text{Tanh}$$

Discriminator architecture was used for CelebA:

$$x \in \mathbb{R}^{64 \times 64 \times 3} \rightarrow \text{Conv}_{64} \rightarrow \text{LeakyReLU}_{0.2} \rightarrow \text{Conv}_{128} \rightarrow \text{BatchNorm} \rightarrow \text{LeakyReLU}_{0.2} \rightarrow \text{Conv}_{256} \rightarrow \text{BatchNorm} \rightarrow \text{LeakyReLU}_{0.2} \rightarrow \text{Conv}_{512} \rightarrow \text{BatchNorm} \rightarrow \text{Tanh}$$

Generator architecture was used for CIFAR10:

$$z \in \mathbb{R}^{128} \rightarrow \text{TransposeConv}_{256} \rightarrow \text{BatchNorm} \rightarrow \text{ReLU} \rightarrow \text{TransposeConv}_{128} \rightarrow \text{BatchNorm} \rightarrow \text{ReLU} \rightarrow \text{TransposeConv}_{64} \rightarrow \text{BatchNorm} \rightarrow \text{ReLU} \rightarrow \text{TransposeConv}_3 \rightarrow \text{Tanh}$$

Discriminator architecture was used for CIFAR10:

$$x \in \mathbb{R}^{32 \times 32 \times 3} \rightarrow \text{Conv}_{64} \rightarrow \text{LeakyReLU}_{0.2} \rightarrow \text{Conv}_{128} \rightarrow \text{BatchNorm} \rightarrow \text{LeakyReLU}_{0.2} \rightarrow \text{Conv}_{256} \rightarrow \text{Tanh}$$

References

- [1] J. Altschuler, J. Niles-Weed, and P. Rigollet. Near-linear time approximation algorithms for optimal transport via Sinkhorn iteration. In *Advances in neural information processing systems*, pages 1964–1974, 2017. (Cited on page 1.)
- [2] M. Arjovsky, S. Chintala, and L. Bottou. Wasserstein generative adversarial networks. In *International Conference on Machine Learning*, pages 214–223, 2017. (Cited on page 1.)
- [3] B. Bhushan Damodaran, B. Kellenberger, R. Flamary, D. Tuia, and N. Courty. Deepjdot: Deep joint distribution optimal transport for unsupervised domain adaptation. In *Proceedings of the European Conference on Computer Vision (ECCV)*, pages 447–463, 2018. (Cited on page 21.)
- [4] N. Bonneel, J. Rabin, G. Peyré, and H. Pfister. Sliced and Radon Wasserstein barycenters of measures. *Journal of Mathematical Imaging and Vision*, 1(51):22–45, 2015. (Cited on page 1.)
- [5] L. Chapel, M. Alaya, and G. Gasso. Partial optimal transport with applications on positive-unlabeled learning. In *Advances in Neural Information Processing Systems 33 (NeurIPS 2020)*, 2020. (Cited on page 7.)
- [6] M. Chen, S. Zhao, H. Liu, and D. Cai. Adversarial-learned loss for domain adaptation. In *Proceedings of the AAAI Conference on Artificial Intelligence*, volume 34, pages 3521–3528, 2020. (Cited on page 12.)
- [7] L. Chizat, G. Peyré, B. Schmitzer, and F.-X. Vialard. Scaling algorithms for unbalanced optimal transport problems. *Mathematics of Computation*, 87(314):2563–2609, 2018. (Cited on pages 6 and 19.)
- [8] L. Chizat, G. Peyré, B. Schmitzer, and F.-X. Vialard. Unbalanced optimal transport: Dynamic and kantorovich formulations. *Journal of Functional Analysis*, 274(11):3090–3123, 2018. (Cited on pages 2 and 3.)

[9] N. Courty, R. Flamary, D. Tuia, and A. Rakotomamonjy. Optimal transport for domain adaptation. *IEEE transactions on pattern analysis and machine intelligence*, 39(9):1853–1865, 2016. (Cited on page 1.)

[10] B. B. Damodaran, B. Kellenberger, R. Flamary, D. Tuia, and N. Courty. Deepjdot: Deep joint distribution optimal transport for unsupervised domain adaptation. In *Proceedings of the European Conference on Computer Vision (ECCV)*, pages 447–463, 2018. (Cited on pages 1, 4, 9, and 12.)

[11] I. Deshpande, Y.-T. Hu, R. Sun, A. Pyrros, N. Siddiqui, S. Koyejo, Z. Zhao, D. Forsyth, and A. G. Schwing. Max-sliced Wasserstein distance and its use for GANs. In *Proceedings of the IEEE Conference on Computer Vision and Pattern Recognition*, pages 10648–10656, 2019. (Cited on page 1.)

[12] P. Dvurechensky, A. Gasnikov, and A. Kroshnin. Computational optimal transport: Complexity by accelerated gradient descent is better than by Sinkhorn’s algorithm. In *ICML*, pages 1367–1376, 2018. (Cited on page 1.)

[13] K. Fatras, T. Sejourne, R. Flamary, and N. Courty. Unbalanced minibatch optimal transport; applications to domain adaptation. In M. Meila and T. Zhang, editors, *Proceedings of the 38th International Conference on Machine Learning*, volume 139 of *Proceedings of Machine Learning Research*, pages 3186–3197. PMLR, 18–24 Jul 2021. (Cited on pages 2, 10, 12, 16, and 21.)

[14] K. Fatras, Y. Zine, R. Flamary, R. Gribonval, and N. Courty. Learning with minibatch Wasserstein: asymptotic and gradient properties. In *AISTATS 2020-23nd International Conference on Artificial Intelligence and Statistics*, volume 108, pages 1–20, 2020. (Cited on pages 2, 4, and 18.)

[15] K. Fatras, Y. Zine, S. Majewski, R. Flamary, R. Gribonval, and N. Courty. Minibatch optimal transport distances; analysis and applications. *arXiv preprint arXiv:2101.01792*, 2021. (Cited on pages 2, 4, and 5.)

[16] J. Feydy, T. Séjourné, F.-X. Vialard, S.-i. Amari, A. Trouve, and G. Peyré. Interpolating between optimal transport and mmd using Sinkhorn divergences. In *The 22nd International Conference on Artificial Intelligence and Statistics*, pages 2681–2690, 2019. (Cited on page 19.)

[17] A. Figalli. The optimal partial transport problem. *Archive for rational mechanics and analysis*, 195(2):533–560, 2010. (Cited on page 6.)

[18] Y. Ganin, E. Ustinova, H. Ajakan, P. Germain, H. Larochelle, F. Laviolette, M. Marchand, and V. Lempitsky. Domain-adversarial training of neural networks. *The Journal of Machine Learning Research*, 17(1):2096–2030, 2016. (Cited on pages 12 and 21.)

[19] A. Genevay, G. Peyré, and M. Cuturi. Learning generative models with Sinkhorn divergences. In *International Conference on Artificial Intelligence and Statistics*, pages 1608–1617. PMLR, 2018. (Cited on pages 2, 4, and 11.)

[20] M. Heusel, H. Ramsauer, T. Unterthiner, B. Nessler, and S. Hochreiter. GANs trained by a two time-scale update rule converge to a local Nash equilibrium. In *Advances in Neural Information Processing Systems*, pages 6626–6637, 2017. (Cited on pages 11 and 21.)

[21] N. Ho, V. Huynh, D. Phung, and M. I. Jordan. Probabilistic multilevel clustering via composite transportation distance. In *AISTATS*, 2019. (Cited on page 1.)

[22] N. Ho, X. Nguyen, M. Yurochkin, H. H. Bui, V. Huynh, and D. Phung. Multilevel clustering via Wasserstein means. In *International Conference on Machine Learning*, pages 1501–1509, 2017. (Cited on page 1.)

[23] J. J. Hull. A database for handwritten text recognition research. *IEEE Transactions on pattern analysis and machine intelligence*, 16(5):550–554, 1994. (Cited on page 12.)

[24] A. Krizhevsky. Learning multiple layers of features from tiny images. Technical report, 2009. (Cited on page 14.)

[25] T. Le, T. Nguyen, N. Ho, H. Bui, and D. Phung. LAMDA: Label matching deep domain adaptation. In *ICML*, 2021. (Cited on page 1.)

[26] Y. LeCun, L. Bottou, Y. Bengio, and P. Haffner. Gradient-based learning applied to document recognition. *Proceedings of the IEEE*, 86(11):2278–2324, 1998. (Cited on page 12.)

[27] T. Lin, N. Ho, and M. Jordan. On efficient optimal transport: An analysis of greedy and accelerated mirror descent algorithms. In *International Conference on Machine Learning*, pages 3982–3991, 2019. (Cited on pages 1 and 9.)

[28] Z. Liu, P. Luo, X. Wang, and X. Tang. Deep learning face attributes in the wild. In *Proceedings of International Conference on Computer Vision (ICCV)*, December 2015. (Cited on page 14.)

[29] M. Long, Z. Cao, J. Wang, and M. I. Jordan. Conditional adversarial domain adaptation. *arXiv preprint arXiv:1705.10667*, 2017. (Cited on page 12.)

[30] Y. Netzer, T. Wang, A. Coates, A. Bissacco, B. Wu, and A. Y. Ng. Reading digits in natural images with unsupervised feature learning. 2011. (Cited on page 12.)

[31] K. Nguyen, N. Ho, T. Pham, and H. Bui. Distributional sliced-Wasserstein and applications to generative modeling. In *International Conference on Learning Representations*, 2021. (Cited on page 1.)

[32] K. Nguyen, S. Nguyen, N. Ho, T. Pham, and H. Bui. Improving relational regularized autoencoders with spherical sliced fused Gromov-Wasserstein. In *International Conference on Learning Representations*, 2021. (Cited on page 1.)

[33] T. Nguyen, Q.-H. Pham, T. Le, T. Pham, N. Ho, and B.-S. Hua. Point-set distances for learning representations of 3D point clouds. In *ICCV*, 2021. (Cited on page 1.)

[34] O. Pele and M. Werman. Fast and robust earth mover’s distance. In *ICCV*. IEEE, 2009. (Cited on page 1.)

[35] X. Peng, B. Usman, N. Kaushik, J. Hoffman, D. Wang, and K. Saenko. Visda: The visual domain adaptation challenge. *arXiv preprint arXiv:1710.06924*, 2017. (Cited on page 12.)

[36] G. Peyré and M. Cuturi. Computational optimal transport: With applications to data science. *Foundations and Trends® in Machine Learning*, 11(5-6):355–607, 2019. (Cited on page 3.)

- [37] T. Salimans, H. Zhang, A. Radford, and D. Metaxas. Improving GANs using optimal transport. In *International Conference on Learning Representations*, 2018. (Cited on pages 11 and 15.)
- [38] J. Solomon, G. Peyré, V. G. Kim, and S. Sra. Entropic metric alignment for correspondence problems. *ACM Transactions on Graphics (TOG)*, 35(4):72, 2016. (Cited on page 1.)
- [39] M. Sommerfeld, J. Schrieber, Y. Zemel, and A. Munk. Optimal transport: Fast probabilistic approximation with exact solvers. *Journal of Machine Learning Research*, 20:105–1, 2019. (Cited on page 2.)
- [40] I. Tolstikhin, O. Bousquet, S. Gelly, and B. Schoelkopf. Wasserstein auto-encoders. In *International Conference on Learning Representations*, 2018. (Cited on page 1.)
- [41] H. Venkateswara, J. Eusebio, S. Chakraborty, and S. Panchanathan. Deep hashing network for unsupervised domain adaptation. In *Proceedings of the IEEE conference on computer vision and pattern recognition*, pages 5018–5027, 2017. (Cited on page 12.)
- [42] C. Villani. *Optimal transport: old and new*, volume 338. Springer, 2009. (Cited on page 3.)